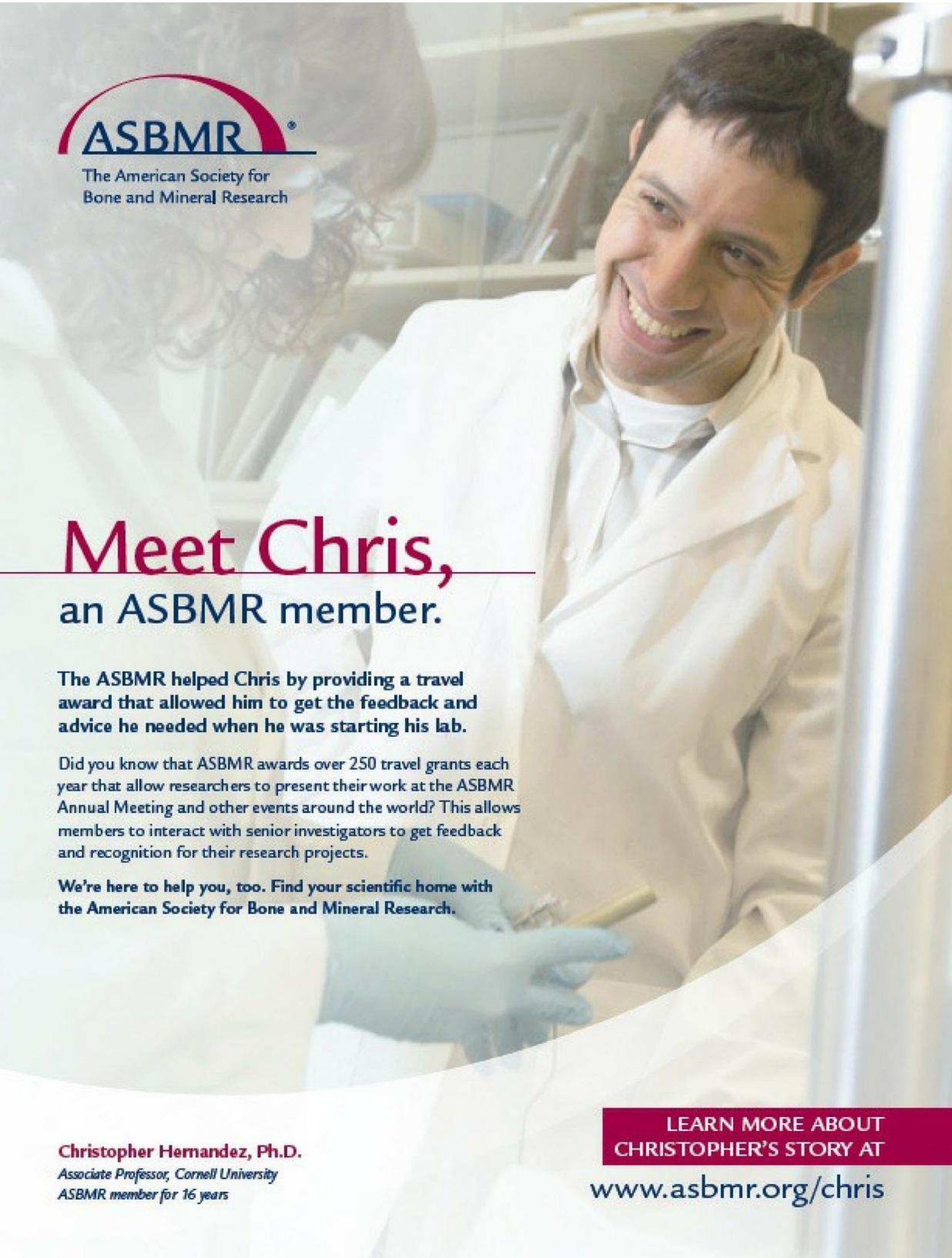

ASBMR®

The American Society for Bone and Mineral Research

Meet Chris, an ASBMR member.

The ASBMR helped Chris by providing a travel award that allowed him to get the feedback and advice he needed when he was starting his lab.

Did you know that ASBMR awards over 250 travel grants each year that allow researchers to present their work at the ASBMR Annual Meeting and other events around the world? This allows members to interact with senior investigators to get feedback and recognition for their research projects.

We're here to help you, too. Find your scientific home with the American Society for Bone and Mineral Research.

Christopher Hernandez, Ph.D.
Associate Professor, Cornell University
ASBMR member for 16 years

LEARN MORE ABOUT CHRISTOPHER'S STORY AT

www.asbmr.org/chris

ORIGINAL ARTICLE

JBMR®

A Complex Role for Lipocalin 2 in Bone Metabolism: Global Ablation in Mice Induces Osteopenia Caused by an Altered Energy Metabolism

Mattia Capulli,[1] Marco Ponzetti,[1] Antonio Maurizi,[1] Sara Gemini-Piperni,[1] Thorsten Berger,[2] Tak Wah Mak,[2] Anna Teti,[1] and Nadia Rucci[1]

[1]Department of Biotechnological and Applied Clinical Sciences, University of L'Aquila, L'Aquila, Italy
[2]The Campbell Family Institute for Breast Cancer Research, Princess Margaret Cancer Centre, University Health Network, Toronto, ON, Canada

ABSTRACT

Lipocalin 2 (Lcn2) is an adipokine that carries out a variety of functions in diverse organs. We investigated the bone phenotype and the energy metabolism of *Lcn2* globally deleted mice (*Lcn2*$^{-/-}$) at different ages. *Lcn2*$^{-/-}$ mice were largely osteopenic, exhibiting lower trabecular bone volume, lesser trabecular number, and higher trabecular separation when compared to wild-type (WT) mice. *Lcn2*$^{-/-}$ mice showed a lower osteoblast number and surface over bone surface, and subsequently a significantly lower bone formation rate, while osteoclast variables were unremarkable. Surprisingly, we found no difference in alkaline phosphatase (ALP) activity or in nodule mineralization in *Lcn2*$^{-/-}$ calvaria osteoblast cultures, while less ALP-positive colonies were obtained from freshly isolated *Lcn2*$^{-/-}$ bone marrow stromal cells, suggesting a nonautonomous osteoblast response to Lcn2 ablation. Given that *Lcn2*$^{-/-}$ mice showed higher body weight and hyperphagia, we investigated whether their osteoblast impairment could be due to altered energy metabolism. *Lcn2*$^{-/-}$ mice showed lower fasted glycemia and hyperinsulinemia. Consistently, glucose tolerance was significantly higher in *Lcn2*$^{-/-}$ compared to WT mice, while insulin tolerance was similar. *Lcn2*$^{-/-}$ mice also exhibited polyuria, glycosuria, proteinuria, and renal cortex vacuolization, suggesting a kidney contribution to their phenotype. Interestingly, the expression of the glucose transporter protein type 1, that conveys glucose into the osteoblasts and is essential for osteogenesis, was significantly lower in the *Lcn2*$^{-/-}$ bone, possibly explaining the in vivo osteoblast impairment induced by the global Lcn2 ablation. Taken together, these results unveil an important role of Lcn2 in bone metabolism, highlighting a link with glucose metabolism that is more complex than expected from the current knowledge. © 2018 American Society for Bone and Mineral Research

KEY WORDS: LCN2; NGAL; BONE METABOLISM; ENERGY METABOLISM; OSTEOBLAST; GLUT1

Introduction

Lipocalin 2 (Lcn2), also known as neutrophil gelatinase-associated lipocalin (NGAL), is a widely expressed protein that has been found to exert many different functions. It belongs to the lipocalin superfamily, which includes at least 20 secreted proteins, such as adipocyte fatty acid binding protein, apolipoprotein D, and retinol-binding protein 4.[1] Lcn2 is involved in inflammation, chronic renal failure, energy metabolism, and tumor development and progression.[2] It is also known to bind matrix metalloproteinase 9 (MMP-9), increasing its stability and thus its activity over time, which is important for neutrophil extravasation and cancer invasion and metastasis. Lcn2 is also classified as an adipokine because it is produced and secreted by adipocytes.[3] Furthermore, a complex and not yet well understood role has recently been suggested for this molecule in the regulation of energy metabolism.[3–8]

We previously showed an involvement of Lcn2 in bone metabolism, pointing to this molecule as a mechanoresponding factor that is upregulated under mechanical unloading in mouse models and in humans.[9,10] Moreover, Lcn2 overexpression reduces osteoblast differentiation and stimulates the production of interleukin 6 (IL-6) and receptor activator of NF-κB ligand (RANKL), which in turn promote osteoclastogenesis.[10]

Based on these findings, we aimed at characterizing the bone phenotype of Lcn2 knockout (*Lcn2*$^{-/-}$) mice, hypothesizing a high bone mass condition. Instead, to our surprise, we found that systemic ablation of *Lcn2* induced a remarkable osteopenic phenotype, due to an impairment of osteoblast differentiation and activity, which conflicts with our previous observation that Lcn2 overexpression impairs osteogenesis.[10] We reconciled these results, demonstrating that the effect of Lcn2 global ablation on bone is caused by an altered energy metabolism rather than by an intrinsic impairment of osteoblast activity. Our data are partially at variance with the observations of Mosialou

Received in original form August 9, 2017; revised form January 29, 2018; accepted February 8, 2018. Accepted manuscript online February 14, 2018.
correspondence to: Nadia Rucci, PhD, Department of Biotechnological and Applied Clinical Sciences, Via Vetoio – Coppito 2, 67100 L'Aquila, Italy.
E-mail: rucci@univaq.it
Additional Supporting Information may be found in the online version of this article.

Journal of Bone and Mineral Research, Vol. 33, No. 6, June 2018, pp 1141–1153
DOI: 10.1002/jbmr.3406

and colleagues,[11] who ruled out any effect of Lcn2 deficiency on the bone phenotype and demonstrated alterations in energy metabolism to some extent different from those observed in our study. We believe that, altogether, the results described so far by us and others suggest that the network of interactions mediated by Lcn2 is extremely complex, requiring further work to be fully elucidated.

Materials and Methods

Materials

Dulbecco's modified minimum essential medium (DMEM), Roswell Park Memorial Institute 1640 (RPMI) medium, α modified Minimum Essential Medium (αMEM), fetal bovine serum (FBS), penicillin, streptomycin, and trypsin were from GIBCO (Uxbridge, UK). Sterile plastic ware was from Falcon Becton-Dickinson (Cowley, Oxford, UK) or Costar (Cambridge, MA, USA). TRIzol reagent, primers and reagents for RT-PCR were from Invitrogen (Carlsbad, CA, USA). The brilliant SYBR Green QPCR master mix was from Stratagene (La Jolla, CA, USA). The infinity hexokinase kit for glucose determination (cat# TR15421) and the osteocalcin (OCN; cat# NC0450271) ELISA kits were from ThermoFisher Scientific (Waltham, MA, USA). The rat/mouse insulin ELISA kit (cat# EZRMI-13K) and the carboxy-terminal cross-linking telopeptide of type 1 collagen (CTX) and mouse tartrate-resistant acid phosphatase (TRAcP) immunoenzymatic kits were from Immunodiagnostic Systems-Nordic Bioscience (Herlev, Denmark). Bone alkaline phosphatase (BALP; cat# MBS281206) ELISA kit was from MyBioSource (San Diego, CA, USA). All the other reagents, including the ALP kit #85 and the TRAcP kit #386, were of the purest grade from Sigma Aldrich Co. (St. Louis, MO, USA).

Animals

Lcn2$^{-/-}$ mice (background C57BL6/J) were generated and kindly provided by Dr. Tak Wah Mak (University Health Network, Toronto, ON, Canada).[12] They are vital, with an overall normal lifespan and fertility. Bone and energy metabolism phenotypes were evaluated at 1, 3, 6, and 12 months of age in wild-type (WT) and *Lcn2*$^{-/-}$ male and female mice. All procedures involving animals and their care were conducted in conformity with national and international laws and policies (European Economic Community Council Directive 86/609, OJ L 358, 1, December 12, 1987; Italian Legislative Decree 4.03.2014, n.26, Gazzetta Ufficiale della Repubblica Italiana no. 61, March 4, 2014) and the Animal Research: Reporting of In Vivo Experiments (ARRIVE) guidelines.

Mice were housed in the animal facility of the University of L'Aquila, Italy, at the following conditions: temperature: 20°C to 24°C, humidity: 60% ± 5%, dark/light cycle: 12/12 hours. They had access to food and water ad libitum and were fed with a standard diet (Mucedola code: 4RF21) composed of 60.8% carbohydrates, 21% proteins, 3.45% fat, 6.8% fibers, 7.95% trace elements, and 12% humidity.

μCT analysis

Images of femurs previously fixed in 4% formaldehyde were acquired using the SkyScan 1174 (Bruker, Billerica, MA, USA) with a resolution of 6.7 μm (X-ray voltage 50 kV). Image reconstruction was carried out employing a modified Feldkamp algorithm,[13] using the Skyscan Nrecon software. Three-dimensional (3D) and two-dimensional (2D) morphometric parameters were calculated for the trabecular bone, 150 slides (4 μm thick) from the growth plate. Threshold values were applied for segmenting trabecular bone corresponding to bone mineral density values of 0.6 mg/cm^3 calcium hydroxyapatite. 3D parameters were based on analysis of a Marching Cubes-type model with a rendered surface.[14] Calculation of all 2D areas and perimeters was based on the Pratt algorithm.[15] Bone structural variables and nomenclature were those suggested by Bouxsein and colleagues.[16]

Bone histomorphometry

Tibias explanted from euthanized WT and *Lcn2*$^{-/-}$ mice were fixed in 4% paraformaldehyde, dehydrated in acetone, and processed for glycol–methacrylate embedding without decalcification. Histomorphometric measurements were carried out on 5-μm-thick sections with an interactive image analysis system (IAS 2000; Delta Sistemi, Rome, Italy)[17] and with the suggested nomenclature.[18] Osteoclast number/bone surface (number/mm^2) and osteoclast surface/bone surface (%) were evaluated after histochemically staining the sections for TRAcP activity. Osteoblast surface/bone surface (%) was evaluated in sections stained with methylene blue/azure II, while dynamic assessment of the mineral apposition rate (MAR) was calculated after double injection of calcein, 10 and 3 days before euthanasia. Bone formation rate (BFR) was calculated according to the following formula: MAR × MS/BA, where MS = mineralized surface and BA = bone area, as suggested by Dempster and colleagues.[18]

Glucose tolerance test

Three-month-old and 12-month-old WT and *Lcn2*$^{-/-}$ mice were subjected to the glucose tolerance test (GTT) following 16 hours of overnight fasting. Briefly, fasted glucose was measured at time 0 using the Accu-Chek Aviva System (Roche Diagnostics, Manheim, Germany) collecting blood directly from the tail, then 2 g/kg of body weight (b.w.) of D-glucose was administered by intraperitoneal (i.p.) injection. Blood glucose and insulin levels were measured 15, 30, 60, and 120 min after D-glucose injection.

Insulin tolerance test

Three-month-old and 12-month-old WT and *Lcn2*$^{-/-}$ mice were subjected to the insulin tolerance test (ITT) after 4 hours of fasting. Briefly, glucose was measured at time 0 using the Accu-Chek Aviva System, then 0.75 U/kg b.w. of recombinant human (rh)-insulin (Humulin®, Eli Lilly and Company, Indianapolis, IN) was administered by i.p. injection. Blood glucose levels were then measured as above after 15, 30, 60, 90, and 120 min after rh-insulin injection.

Glucose-stimulated insulin secretion by primary pancreatic islets

Primary pancreatic islets were isolated from 3-month-old male mice by intraductal injection of 3 mL of collagenase P solution, according to Li and colleagues,[19] then pancreatic islets were recovered and cultured in RPMI medium containing 11mM glucose and 10% FBS.

Seven to 10 islets were transferred in 24-well plates and glucose-starved by incubation in Krebs Ringer bicarbonate HEPES buffer (114mM NaCl; 4.7mM KCl; 1.16mM $MgSO_4$; 1.2mM KH_2PO_4; 2.5mM $CaCl_2$; 5mM $NaHCO_3$; 20mM HEPES; 0.2% BSA)

for 45 min at 37°C. Then, the islets were incubated at 37°C in Krebs Ringer bicarbonate HEPES buffer containing 5.5mM or 16mM glucose. After 1 hour, the medium was harvested and centrifuged at 250*g* for 5 min. The supernatants were used to quantify the secreted insulin by ELISA kit, while the pellets were lysed to isolate the DNA. Insulin secretion was then normalized versus the DNA content.

Experiments in metabolic cages

Mice were acclimated for 48 hours in the experimental room, then transferred into metabolic cages (one mouse per cage) to measure food intake, water intake, and urine output. All experiments were run on a 10-hour light/14-hour dark cycle.

Food intake was evaluated for 4 and 21 days.[20] Briefly, 15 ± 0.1 g of food was given to each mouse at the start of every light cycle. At the end of the light cycle, food was weighted again, then the difference between the starting weight and the final weight was computed to measure the food intake. This value was also used as a starting weight to determine the night cycle food intake. After one light/dark cycle, the food left in the cages was changed with 15 ± 0.1 g of fresh food.

Water intake was measured each day at the start of every light cycle. Briefly, 50 g of drinking water was weighted and given to the mice in a water bottle. At the start of the next light cycle, water weight was measured again, accounting for the water dripped out of the bottle, which was also collected by the metabolic cage, giving the amount of water drank by the mice. This value was then converted to milliliters by measuring the density of the water with an analytical scale and micropipettes.

Urine was also collected, using the built-in system of the metabolic cages. Urine volumes were measured at the end of every dark and light cycle. Urine volumes were then centrifuged at 500*g* for 15 min and supernatants were deep frozen at –80°C until use.

Glucose concentration in urine

The concentration of glucose in the urine collected from WT and *Lcn2*$^{-/-}$ mice at the end of the dark cycles was evaluated using the Infinity hexokinase-based glucose detection kit, according to the manufacturer's instructions.

Insulin, bone turnover biomarker, and Lcn2 concentrations in sera

Sera from WT and *Lcn2*$^{-/-}$ mice were used for detection of insulin, bone turnover biomarker (CTX, TRAcP, BALP, OCN), and Lcn2 concentrations by ELISA kits, according to the manufacturers' instructions.

Osteoblast primary cultures

Calvarias from 7-day-old WT and *Lcn2*$^{-/-}$ mice were explanted, cleaned free of soft tissues, and digested three times with 1 mg/mL *Clostridium histolyticum* type IV collagenase and 0.25% trypsin, for 20 min at 37°C, with gentle agitation. Cells from the second and third digestions were plated and grown in standard conditions, in DMEM plus 10% FBS. At confluence, cells were trypsinized and plated according to the experimental protocol. The purity of the culture was evaluated by the expression of the osteoblast biomarkers, ALP, Runx-2, PTH/PTH related peptide receptor, type I collagen, and OCN and by the histochemical evaluation of ALP activity.

Mineralization assay

Osteoblast standard medium was supplemented with 10mM β-glycerophosphate and 50 μg/mL ascorbate (osteogenic medium). Osteoblasts were cultured for 3 weeks before evaluation of mineralization by von Kossa staining.

ALP-positive colony forming unit assay

Femurs and tibias of 7-day-old WT or *Lcn2*$^{-/-}$ mice were cleaned out of soft tissues, chopped with a sterile blade, and bone marrow cells were flushed out and pulled together. Cells were pelleted at 350*g* for 10 min and then 500,000 cells were plated in 6-cm dishes with osteogenic medium. Medium was changed every 5 days. At the 14th day, cells were fixed in 4% paraformaldehyde and histochemically stained for ALP. Pictures were taken with a complementary metal-oxide semiconductor (CMOS) camera and the number and area of ALP-positive colonies were analyzed to estimate the amount of osteoblast progenitors in the bone marrow.

Osteoclast primary cultures

Femurs and tibias of 7-day-old WT or *Lcn2*$^{-/-}$ mice were cleaned of soft tissues, chopped with a sterile blade, and bone marrow was flushed out, diluted 1:1 in Hank's balanced salt solution (HBSS), layered over Histopaque 1077 solution, and centrifuged at 400*g* for 30 min. Buffy coat cells were collected, washed twice with HBSS, resuspended in DMEM plus 10% FBS, and plated in culture dishes at a density of 1×10^6 cells/cm^2. After 3 hours, cell cultures were washed with PBS to remove nonadherent cells and maintained for 7 days in the same medium supplemented with 50 ng/mL rh-macrophage-colony stimulating factor (rhM-CSF) and 120 ng/mL rhRANKL. Mature osteoclasts and committed precursors were detected by TRAcP histochemical staining.

Adipocyte isolation

Primary adipocytes were isolated from the gonadal (epididymal) white adipose tissue of 2-month-old male mice. Briefly, gonadal fat pad was collected and kept in the Adipo Buffer (120mM NaCl; 6mM KCl; 1.2mM $MgSO_4$; 1mM $CaCl_2$; 0.6mM Na_2HPO_4; 0.4mM NaH_2PO_4; 20mM HEPES) supplemented with 1% BSA and 1mM D-glucose. The tissue was digested using 2 mg of collagenase P per each gram of fat, for 1 hour at 37°C. Adipocytes were purified by serial centrifugations (180*g* for 3 min, three times) and plated in αMEM supplemented with 1% FBS. After 1 hour, the adipocytes were collected and processed for RNA extraction.

Comparative real-time RT-PCR

Total RNA was extracted from mouse tissues and from osteoblast and adipocyte cultures, using the TRIzol® method. One microgram (1 μg) of total RNA was reverse transcribed into cDNA using Moloney Murine Leukemia Virus (M-MLV) reverse transcriptase and the equivalent of 0.1 μg was processed using the Brilliant® SYBR® Green QPCR master mix for real-time PCR or Thermo Scientific 2X greentaq mastermix for conventional PCR. Results, expressed as fold increase, were normalized versus the housekeeping gene *Gapdh*.

Statistics

Results were expressed as the mean ± SD of at least three independent experiments or three to 10 mice/group, as specified in the figure legends. Results from the two sexes

were analyzed separately. The sex is specified in the figure legends. Statistical analyses were performed using the unpaired Student's *t* test, conducted either on raw data or on the area under the curve, according to the type of data. The statistical method is indicated in the figure legends. A p value <0.05 was conventionally considered statistically significant.

Results

Bone metabolism

We previously showed that increased Lcn2 expression, in response to bone mechanical unloading, impaired in vitro osteoblast differentiation, and enhanced osteoblast RANKL expression and subsequent osteoclast formation.[10] To thoroughly characterize the role of Lcn2 in bone metabolism, we investigated the bone phenotype of *Lcn2* globally deleted mice hypothesizing an enhanced osteogenesis compared to WT mice. As expected, our *Lcn2*$^{-/-}$ mice did not express Lcn2 mRNA (Supporting Fig. 1A) and protein (Supporting Fig. 1B) in any tissue investigated. Consistently, circulating Lcn2 was undetectable (Supporting Fig. 1C).

The longitudinal growth of the skeleton of *Lcn2*$^{-/-}$ mice appeared normal, as shown by gross observations and measurement of the femur length (Supporting Fig. 1D). However, to our surprise, μCT analysis revealed that the trabecular bone volume over tissue volume was dramatically lower in *Lcn2*$^{-/-}$ compared to WT mice at all ages analyzed (Fig. 1*A*,*B*). Consistently, evaluation of trabecular parameters revealed a significantly lower trabecular number (Fig. 1*C*), whereas trabecular thickness was slightly higher in *Lcn2*$^{-/-}$ mice at 1 month of age, but did not show differences with WT mice at the other ages (Fig. 1*D*). A higher trabecular separation was observed in *Lcn2*$^{-/-}$ mice (Fig. 1*E*), whereas the cortical thickness was significantly lower only in elderly *Lcn2*$^{-/-}$ mice (Fig. 1*F*). Interestingly, the trabecular bone variables in the L_4 vertebrae showed no difference between WT and *Lcn2*$^{-/-}$ mice at 3 months of age (Supporting Fig. 1E). This observation was consistent with the report by Mosialou and colleagues,[11] who found no vertebral phenotype either in global or osteoblast-specific Lcn2 ablated mice at this age. However, we observed a significant reduction of the bone volume in the L_4 vertebrae of older mice (12 months old) (Supporting Fig. 1E–H), suggesting a delayed loss of bone mass in this bone segment.

To determine whether these differences in the bone structural variables were due to osteoblastic and/or osteoclastic dysfunctions, we performed histomorphometric analysis of distal femur secondary spongiosa and observed that osteoblast number and surface over bone surface were significantly lower in *Lcn2*$^{-/-}$ mice compared to WT littermates (Fig. 2*A*–*C*). Consistently, double calcein labeling (Fig. 2*D*) showed reduced bone formation rate and MAR in the *Lcn2*$^{-/-}$ mice (Fig. 2*E*,*F*). In contrast, no modulation of the osteoclast variables was observed (Fig. 2*G*–*I*), suggesting that the osteopenic phenotype of the *Lcn2*$^{-/-}$ mice was dependent on the osteoblasts.

In agreement with this hypothesis, lower serum levels of BALP (Fig. 2*J*) and OCN (Fig. 2*K*) were observed in *Lcn2*$^{-/-}$ mice, while the serum osteoclast and bone resorption biomarkers, TRAcP (Fig. 2*L*) and CTX (Fig. 2*M*), respectively, were unremarkable. Finally, real-time RT-PCR in *Lcn2*$^{-/-}$ marrow-depleted femurs showed a significant reduction of *Alp*, *Runx2*, and *Col1A2* compared to WT mice (Fig. 2*N*).

The bone loss found in *Lcn2*$^{-/-}$ mice was unexpected as it conflicted with our previous observation that Lcn2 was increased in mechanically unloaded osteopenic mice.[10] To understand the mechanisms underlying this discrepancy, we first investigated which cell types expressed Lcn2 in the bone. Interestingly, we found low transcriptional levels of Lcn2 in marrow-depleted bones compared to the bone marrow alone and to the whole bone (Supporting Fig. 2A). Moreover, in cultured primary calvaria osteoblasts, we observed faint levels of Lcn2 mRNA compared to marrow cells (Supporting Fig. 2B) and primary adipocytes (Supporting Fig. 2C). Similar results were observed detecting the Lcn2 protein in bone and gonadal fat sections by immunohistochemistry, with a positive signal found in marrow cells and adipocytes but not in osteoblasts (Supporting Fig. 2D). These results confirmed previous observations[9,10,21] but are at variance with the data reported by Mosialou and colleagues,[11] who found a basal osteoblast expression of Lcn2 10-fold higher than in the other Lcn2-expressing organs.

Given the complexity of the in vivo results, we next assessed whether the cellular changes observed in the *Lcn2*$^{-/-}$ mice were cell-autonomous by evaluating the bone cell phenotype in vitro. Primary osteoclasts, differentiated from the bone marrow–derived mononuclear cell fraction, showed no differences in formation or function (Fig. 3*A*,*B*). This was inconsistent with the results of Hyun-Ju and colleagues,[22] who found more and larger osteoclasts in the bone marrow cultures of another model of *Lcn2*$^{-/-}$ mouse. Surprisingly, in contrast with the in vivo data, osteoblasts isolated from WT and *Lcn2*$^{-/-}$ calvarias exhibited similar levels of ALP activity (Fig. 3*C*), with no differences in the ability to mineralize the extracellular matrix (Fig. 3*D*) and in the transcriptional expression of *Alp* (Fig. 3*E*) and *Runx2* (Fig. 3*F*). Because these assays can only be performed after various days of culture, which deprive the cells of environmental factors present in vivo, we speculated that the in vivo global Lcn2 ablation affected osteoblasts by an indirect mechanism.

Consistent with this assumption, Lcn2 silencing of cultured osteoblasts by the means of specific siRNA (Supporting Fig. 3A) did not influence *Alp* and *Runx2* (Supporting Fig. 3B,C), in agreement with the observation that our osteoblasts expressed very low basal levels of Lcn2[9,10,21] (Supporting Fig. 2). In contrast, a colony forming unit assay, which gives an instant picture of the in vivo situation detecting the ALP-positive osteoblast precursor pool in the freshly harvested bone marrow, showed significantly lower ALP-positive colony number (Fig. 3*G*) and area (Fig. 3*H*) in the *Lcn2*$^{-/-}$ cultures, suggesting that global Lcn2 ablation in vivo reduced the number of osteoblast precursors in the bone marrow. From this set of data, we concluded that the impaired osteoblast activity in *Lcn2*$^{-/-}$ mice was not cell-autonomous. These results could also reconcile our seemingly contradictory observations that both Lcn2 overexpression[10] and ablation (this study) impair osteogenesis, because the former could affect osteoblasts by a direct mechanism, while the latter could act through an indirect process involving a systemic regulation.

Energy metabolism

Given that bone and energy metabolism are tightly linked,[23] we investigated whether the energy metabolism was disturbed in *Lcn2*$^{-/-}$ mice, thus indirectly affecting the bone phenotype. We noticed that *Lcn2*$^{-/-}$ mice were bigger in size compared to matched WT littermates, in agreement with the observation of Mosialou and colleagues.[11] The body weight (Fig. 4*A*) and the weight of the gonadal fat (Fig. 4*B*, Supporting

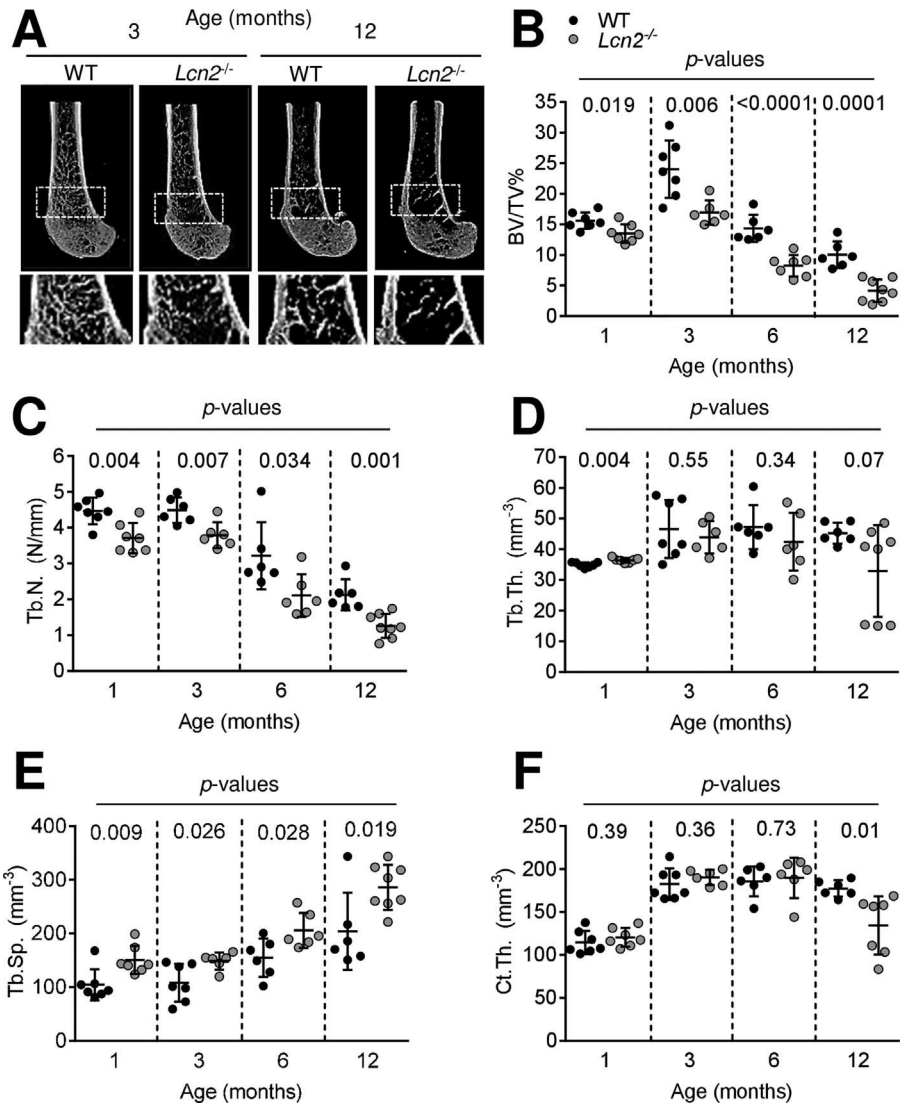

Fig. 1. *Lcn2*$^{-/-}$ mice show an osteopenic phenotype. μCT analysis of distal femur secondary spongiosa of WT and *Lcn2*$^{-/-}$ male mice. (*A*) Representative images of femurs analyzed at the indicated ages. (*B*) BV/TV (%) and (*C*) Tb.N, (*D*) Tb.Th, and (*E*) Tb.Sp. (*F*) Ct.Th (unpaired Student's *t* test; number of mice/group = 6 to 7). BV/TV = bone volume/total tissue volume; Tb.N = trabecular number; Tb.Th = trabecular thickness; Tb.Sp = trabecular separation; Ct. Th = cortical thickness.

Fig. 4A) were significantly higher in *Lcn2*$^{-/-}$ compared to WT mice at all ages evaluated. The *Lcn2*$^{-/-}$ gonadal white adipose tissue showed more adipocytes (Fig. 4*C*), while the adipocyte area/tissue area was similar in the two genotypes (Fig. 4*D*). The higher body weight was likely due to a greater food intake in *Lcn2*$^{-/-}$ compared to WT mice, measured at 3 months (Fig. 4*E*,*F*) and 12 months of age (Supporting Fig. 4B,C). These results were consistent with the observations of Mosialou and colleagues.[11]

To assess whether these features could be associated with an altered glucose metabolism, we measured the glycemia and observed that *ad libitum*–fed circulating glucose concentration was similar in the two genotypes, while fasted glucose was significantly lower in *Lcn2*$^{-/-}$ mice (Fig. 5*A*). Consistently, dynamic measurements of glycemia by GTT confirmed lower blood glucose in the *Lcn2*$^{-/-}$ versus the WT mice (Fig. 5*B*), while insulin levels measured at each time point were comparable (Supporting Fig. 5A) and ITT showed no differences in the sensitivity to insulin (Fig. 5*C*).

To investigate the energy metabolism more deeply, and because insulin is also important for bone metabolism,[23,24] we evaluated the insulinemia and observed that it was significantly higher in *Lcn2*$^{-/-}$ mice compared to WT mice, under feeding conditions (Fig. 5*D*). This was at variance with the report of Mosialou and colleagues[11] on conditional osteoblast *Lcn2*$^{-/-}$ mice, which showed a significant lower serum insulin level compared to control mice. In our mice, histological examination of endocrine pancreas showed a similar number of Langerhans islets in the two genotypes (Fig. 5*E*), although the islets were larger in 3-month-old *Lcn2*$^{-/-}$ compared to WT mice (Fig. 5*F*), as confirmed also by immunofluorescence for insulin (Fig. 5*G*). A similar result was reported by Mosialou and colleagues[11] in osteoblast-specific *Lcn2*-ablated mice, while such an analysis was not performed in the global *Lcn2*$^{-/-}$ model. To better clarify

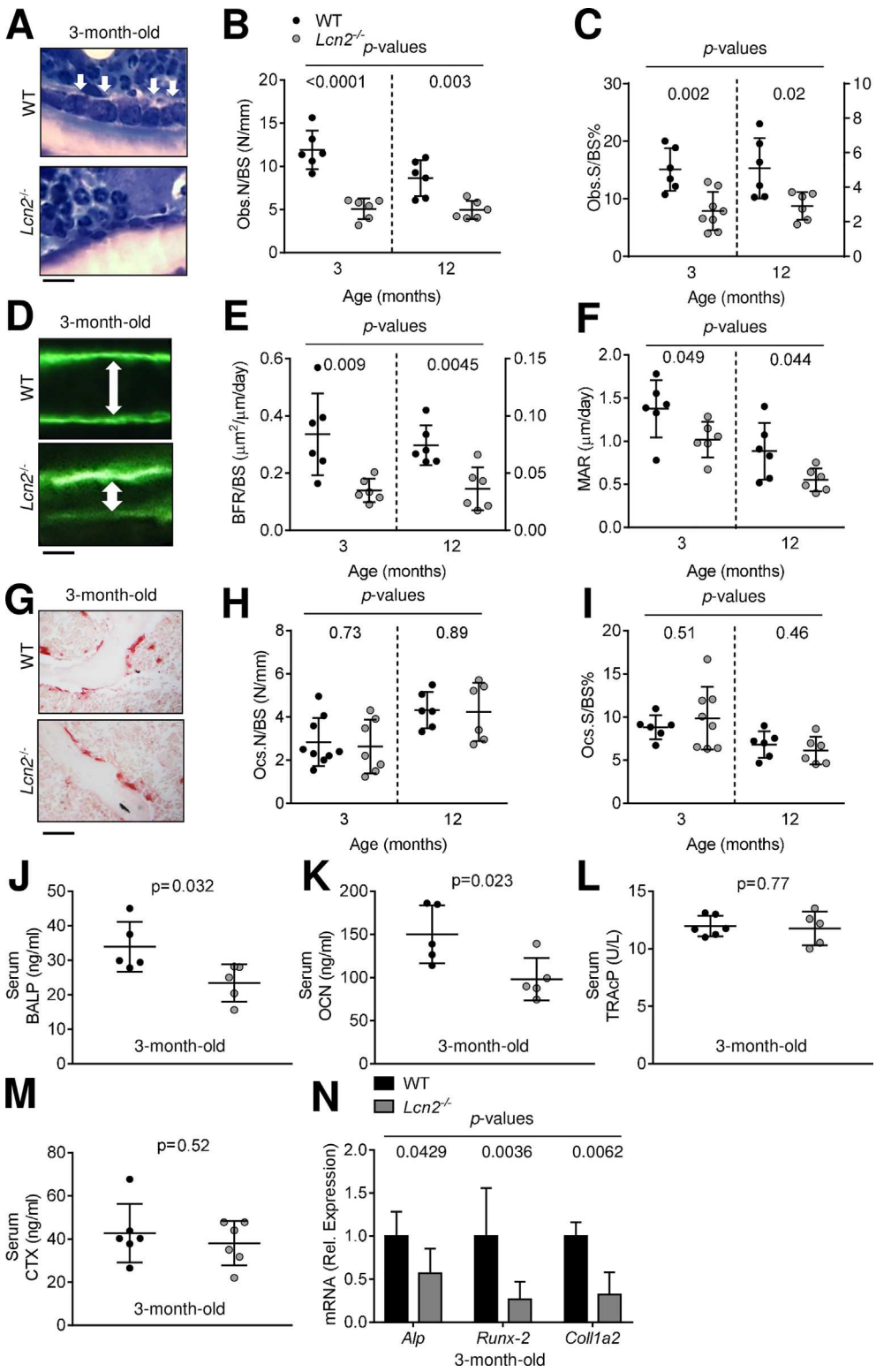

Fig. 2. Histomorphometry and bone turnover biomarkers in WT and *Lcn2*$^{-/-}$ mice. (*A*) Histological sections from WT and *Lcn2*$^{-/-}$ male mouse proximal tibias stained with methylene blue/azure II to evaluate (*B*) Ob.N/BS and (*C*) Ob.S/BS; arrows = osteoblasts, scale bar = 5 μm. (*D*) Double in vivo calcein labeling (green fluorescence; scale bar = 5 μm) and evaluation of (*E*) BFR/BS and (*F*) MAR. (*G*) Histological sections of proximal tibias subjected to TRAcP histochemical assay to evaluate (*H*) Oc.N and (*I*) Oc.S/BS; scale bar = 10 μm. (*J,K*) Serum analysis of the bone formation biomarkers (*J*) BALP and (*K*) OCN. (*L,M*) Serum analysis of (*L*) TRAcP and (*M*) CTX. (*N*) Transcriptional expression of *Alp*, *Runx2*, and *Collagen 1A2* in femurs (unpaired Student's *t* test, number of mice/group = 5 to 8). Ob.N/BS = osteoblast number/bone surface; Ob.S/BS = osteoblast surface/bone surface; BFR/BS = bone formation rate/bone surface; MAR = mineral apposition rate; Oc.N = osteoclast number; Oc.S/BS = osteoclast surface/bone surface; BALP = bone alkaline phosphatase; OCN = osteocalcin.

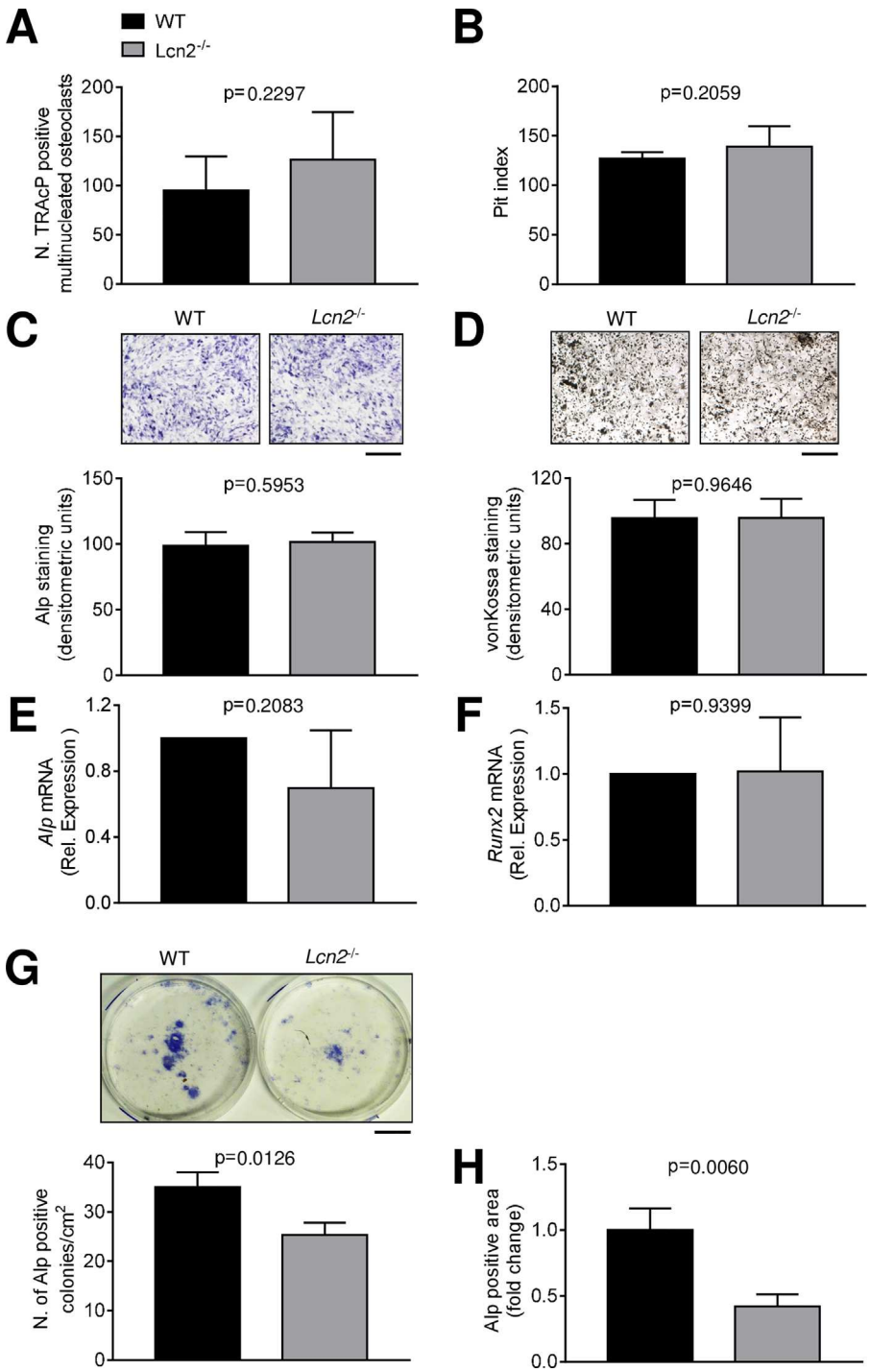

Fig. 3. Effect of *Lcn2* ablation on osteoclast and osteoblast phenotype. (*A*,*B*) Purified bone marrow mononuclear cells from 7-day-old WT and *Lcn2*$^{-/-}$ mice were allowed to differentiate in osteoclasts in the presence of 25 ng/mL rhM-CSF and 120 ng/mL rhRANKL. (*A*) At the end of the experiment, mature osteoclasts were detected by TRAcP histochemical staining and counted. (*B*) Purified bone marrow mononuclear cells were plated onto bone slices and allowed to differentiate as described in *A*. At the end of the experiment, bone slices were stained with toluidine blue and the pit index calculated. (*C*–*F*) Primary osteoblasts were isolated from the calvariae of 7-day-old WT and *Lcn2*$^{-/-}$ mice after 3 digestions with 1 mg/mL *Clostridium histolyticum* type IV collagenase and 0.25% trypsin. (*C*) ALP activity evaluated by histochemical assay (inset; scale bar = 50 μm) and quantified by densitometric analysis (graph). (*D*) Von Kossa staining (inset; scale bar = 50 μm) of mineralization nodules from WT and *Lcn2*$^{-/-}$ primary osteoblasts cultured in standard medium supplemented with 10mM β-glycerophosphate and 50 μg/mL ascorbic acid (osteogenic medium) for 3 weeks. (*E*,*F*) Transcriptional expression of (*E*) *Alp* and (*F*) *Runx2*. (*G*,*H*) Osteogenic colony forming unit assay performed in bone marrow stromal cells flushed out from femurs of 7-day-old WT and *Lcn2*$^{-/-}$ mice. Evaluation of (*G*) number of ALP-positive colonies and (*H*) ALP-positive area; scale bar = 1 mm. Results are the mean ± SD of three independent experiments (unpaired Student's *t* test).

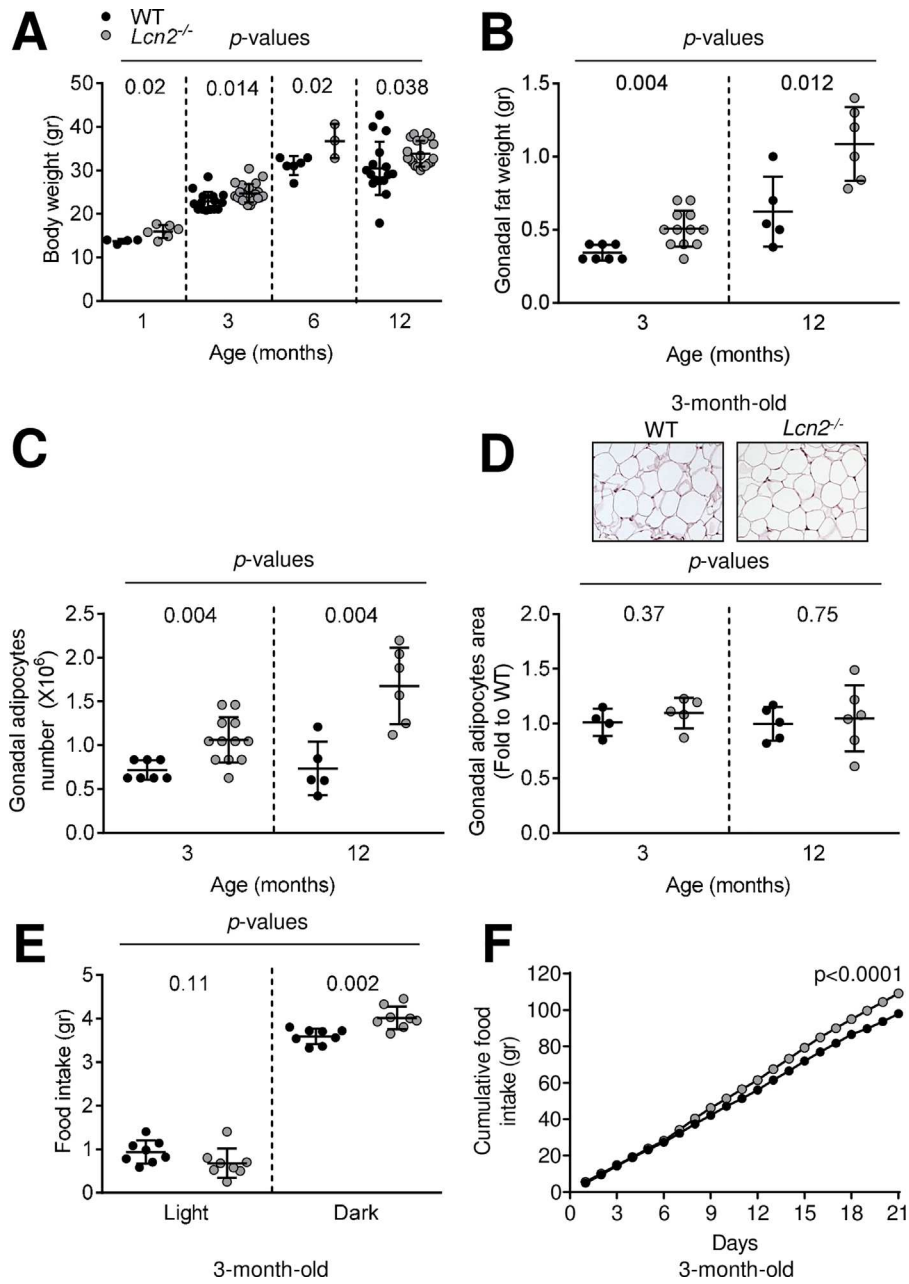

Fig. 4. *Lcn2*$^{-/-}$ mice show increased body and gonadal fat weight. (*A*) Body weight measurements in WT and *Lcn2*$^{-/-}$ male mice at the ages indicated in the *x* axis. (*B–D*) Three-month-old and 12-month-old WT and *Lcn2*$^{-/-}$ male mice were euthanized, then gonadal fat was collected and (*B*) weighed. (*C*) Evaluation of gonadal adipocyte cell number. (*D*) Histological sections of gonadal fat from WT and *Lcn2*$^{-/-}$ mice stained with hematoxylin/eosin (inset; scale bar = 50 μm) and quantification of the adipocyte area. (*E,F*) Three-month-old WT and *Lcn2*$^{-/-}$ mice were housed in metabolic cages to evaluate food intake after (*E*) 4 days and (*F*) 21 days (unpaired Student's *t* test, number of mice/group = 3 to 10).

this phenotype, we performed a glucose-stimulated insulin secretion (GSIS) test in ex vivo pancreatic islets freshly isolated from WT and *Lcn2*$^{-/-}$ mice and observed a greater release of insulin from *Lcn2*$^{-/-}$ islets after exposure to both normal and high glucose concentrations (Fig. 5*H*).

We next evaluated the energy metabolism phenotype in elderly mice (12 months) and observed a trend to lower fasted glucose in the *Lcn2*$^{-/-}$ genotype (Fig. 5*I*). Similarly, GTT still showed lower glucose levels in *Lcn2*$^{-/-}$ mice (Fig. 5*J*), while insulin sensitivity remained similar in the two genotypes (Fig. 5*K*). Insulinemia was significantly higher in 12-month-old *Lcn2*$^{-/-}$ mice also (Fig. 5*L*), while neither number nor area of pancreatic islets were changed (Fig. 5*M,N*). Lower levels of fasted glucose were also observed in both adult and aged female *Lcn2*$^{-/-}$ mice (Supporting Fig. 5B), paralleled also in this sex by a significant increase of glucose tolerance (Supporting Fig. 5C,D).

Kidney alterations

To establish whether kidney alterations could contribute to the *Lcn2*$^{-/-}$ mouse phenotype, we measured the urine output in metabolic cage experiments. We found polyuria in *Lcn2*$^{-/-}$ mice

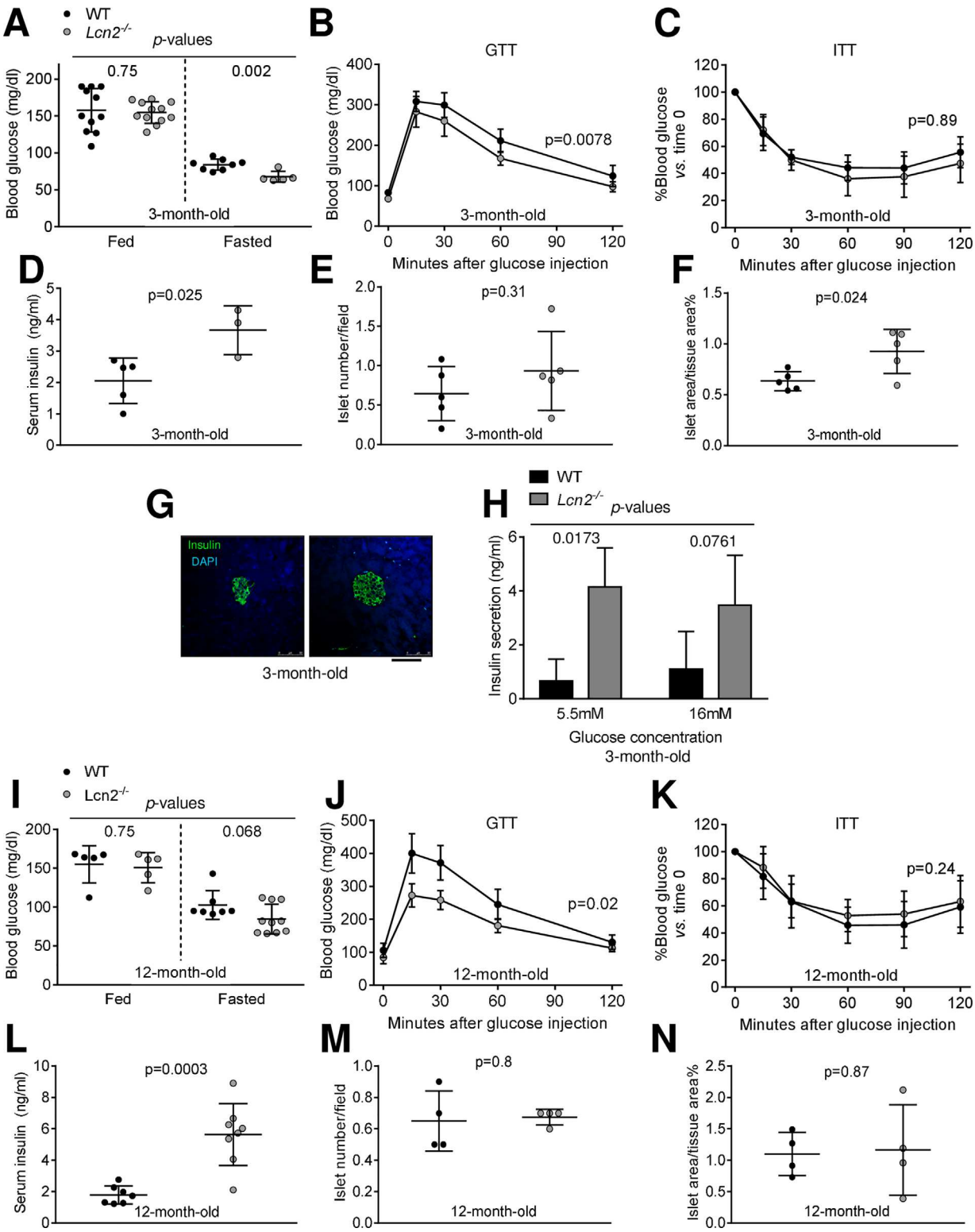

Fig. 5. Effect of *Lcn2* ablation on energy metabolism. (*A–H*) Three-month-old WT and *Lcn2*$^{-/-}$ male mice were evaluated (*A*) for their glucose levels under ad libitum feeding and fasting conditions. (*B*) WT and *Lcn2*$^{-/-}$ mice were injected i.p. with 2 g/kg body weight of glucose and subjected to GTT at the times indicated in the abscissa. (*C*) WT and *Lcn2*$^{-/-}$ mice were injected with 0.75 UI/kg body weight of Humulin® (rhInsulin) and subjected to ITT at the times indicated in the abscissa. (*D*) ELISA assay to assess serum levels of insulin. (*E*) Pancreatic islet number and (*F*) area over tissue area. (*G*) Immunofluorescence analysis of insulin in sections from pancreas of WT and *Lcn2*$^{-/-}$ mice; scale bar = 50 μm. (*H*) GSIS test in pancreatic islets isolated from 3-month-old WT and *Lcn2*$^{-/-}$ male mice. (*I*) Twelve-month-old WT and *Lcn2*$^{-/-}$ male mice were evaluated for their glucose levels under ad libitum feeding and fasting conditions. (*J*) Glucose and (*K*) insulin tolerance test. (*L*) Serum levels of insulin. (*M*) Pancreatic islet number and (*N*) area over tissue area (unpaired Student's *t* test, number of mice/group = 4 to 11).

at both 3 and 12 months of age (Fig. 6*A*), while their water intake was similar to WT mice (Fig. 6*B*,*C*). Interestingly, glycosuria was also observed in *Lcn2*$^{-/-}$ mice (Fig. 6*D*), likely associated with the polyuria described in Figure 6*A*. Moreover, Lcn2 has been previously associated with chronic kidney disease progression in mice and humans[25] and *Lcn2*$^{-/-}$ mice showed proteinuria (Fig. 6*E*) and histological signs of renal cortex vacuolization (Fig. 6*F*,*G*), thus suggesting the development of kidney injury and its potential involvement in the circulating glucose depletion observed in the *Lcn2*$^{-/-}$ mice.

Molecular mechanism

To investigate the effect of Lcn2 deletion on the overall insulin signaling, we performed Western blot analysis for the activated (ie, phosphorylated) insulin receptor (InsR) and its downstream target AKT in gonadal white adipose tissue, quadriceps, and femur protein lysates. Phosphorylation of InsR and AKT did not appear different between the two genotypes in quadriceps and femurs. In gonadal white adipose tissue, we observed a significant increase of InsR phosphorylation and a trend of increase of AKT phosphorylation (Supporting Fig. 6A–D, left panels), suggesting that the high circulating insulin in *Lcn2*$^{-/-}$ mice targets especially the white adipose tissue. These results ruled out that the bone phenotype of *Lcn2*$^{-/-}$ mice was associated with altered insulin signaling and led us to hypothesize that a specific glucose-associated alteration could affect the bone.

To address this hypothesis, we evaluated the expression of GLUT1, which is the transporter through which glucose enters the osteoblasts by an insulin-independent mechanism, driving osteoblast differentiation and bone deposition.[26] *Glut1* transcriptional expression was lower in marrow depleted femurs from *Lcn2*$^{-/-}$ mice compared to WT, while it was higher in *Lcn2*$^{-/-}$ liver (Fig. 7*A*) as expected from the insulin-induced hypoglycemic phenotype.[27] The lower level of GLUT1 in the marrow-depleted bone was also confirmed by Western blot (Fig. 7*B*). Taken together, these results suggest that Lcn2 global ablation prevents the full expression of a glucose transporter that is essential for osteogenesis,[26] at least in part explaining the osteopenic phenotype observed in the *Lcn2*$^{-/-}$ mice.

Discussion

Lcn2 is a versatile protein involved in many complex and often contradictory functions (Supporting Table 1). In our work, we showed that *Lcn2*$^{-/-}$ mice had a marked osteopenic phenotype due to reduced osteoblast number and activity, with no changes in osteoclast parameters. Our data supports the concept that this phenotype was not primary, but secondary to deregulated energy metabolism and, at least in part, due to the impairment of the GLUT1 expression in the *Lcn2*$^{-/-}$ bone. Accordingly, differentiation and in vitro mineralization ability of cultured calvarial osteoblasts were similar between WT and *Lcn2*$^{-/-}$ cells, thus suggesting an in vivo non–cell autonomous osteoblast response to Lcn2 ablation. In vitro osteoclast function and gene expression were also similar in the WT and *Lcn2*$^{-/-}$ genotypes. This is at variance with a recent report which proposed that *Lcn2*$^{-/-}$ mice had no bone phenotype in vivo, while in vitro osteoclasts were larger and their osteoclast precursors proliferated more due to upregulation of the M-CSF receptor, c-Fms.[22] This result is surprising, further strengthening the complexity of the Lcn2 pathway in the bone.

The involvement of energy metabolism reconciles this study with our previous work,[10] in which we showed impaired osteoblast function when Lcn2 was overexpressed in unloading conditions. This paradox could depend on the fact that overexpression of Lcn2 could have a direct negative influence on osteoblasts, while in our global Lcn2 ablated mice the negative effect on osteoblasts could be mediated by a complex alteration of energy metabolism and kidney function.

Our results on the bone phenotype also diverge from those described in the elegant report by Mosialou and colleagues,[11] who found normal bone mass in both global and osteoblast-specific Lcn2-deleted mice, and normal circulating levels of OCN in osteoblast-specific–deleted mice, concluding that the effect of Lcn2 deletion was not on the bone but only on appetite in the brain. These discrepancies could be explained by the fact that Mosialou and colleagues[11] investigated the bone phenotype only in the vertebras and only at 3 months of age. Concordantly, also the vertebral phenotype of our 3-month-old global *Lcn2*$^{-/-}$ mice was unremarkable, while vertebral low bone mass was apparent in older mice. In contrast, we observed long-bone osteopenia at all ages, representing another piece of complexity in the Lcn2 pathway, which seems to exhibit both time-based and site-based diversities.

Another important difference between these two studies was in the osteoblast basal expression of Lcn2. Mosialou and colleagues[11] showed a very high Lcn2 level in WT osteoblasts, 10-fold more than in adipocytes. This is at variance with previous reports, which showed that Lcn2-producing cells are mainly adipocytes and bone marrow cells[1–8,10,21] rather than osteoblasts.[28,29] In Mosialou and colleagues,[11] the bone marrow was not included in the transcriptional and protein analyses, while in our previous work, we showed that the marrow Lcn2–highly expressing cells did not belong to the stromal compartment, thus ruling out the osteoblast lineage.[9,10,21] This observation was complemented in this study, in which high Lcn2 expression was detected immunohistochemically in marrow cells and in gonadal adipocytes but not in endosteal cells, confirming previous reports.[1–8,10,21,28,29] Unfortunately, we are not able to provide a credible explanation for the divergences with the results of Mosialou and colleagues,[11] which can only be clarified by future research.

The role of Lcn2 in the energy metabolism has been investigated by various groups, but again the results did not fully clarify the exact pattern, and studies diverge in their observations and conclusions (Supporting Table 1). The fact that our *Lcn2*$^{-/-}$ mice had an altered control of energy metabolism was suggested by their hyperphagia and mild obesity. The adipose tissue was clearly affected by the *Lcn2* deletion with an increase of the number of adipocytes and of the signaling response to insulin. We also showed that *Lcn2*$^{-/-}$ mice exhibited fasted hypoglycemia and greater glucose tolerance but, at variance with Mosialou and colleagues[11] and other reports,[6] we observed a fed hyperinsulinemia, corroborated by the detection of bigger pancreatic islets in *Lcn2*$^{-/-}$. Increased insulin secretion was confirmed by the GSIS test in isolated starved *Lcn2*$^{-/-}$ islets exposed to glucose; therefore, we are confident that, in our experimental condition, hyperinsulinemia characterizes the *Lcn2*$^{-/-}$ mouse energy phenotype. This hyperinsulinemia could be associated with the mild obesity observed in the *Lcn2*$^{-/-}$ mice, in agreement with reports that showed a causal association between these two conditions.[27] In fact, it has been proposed that

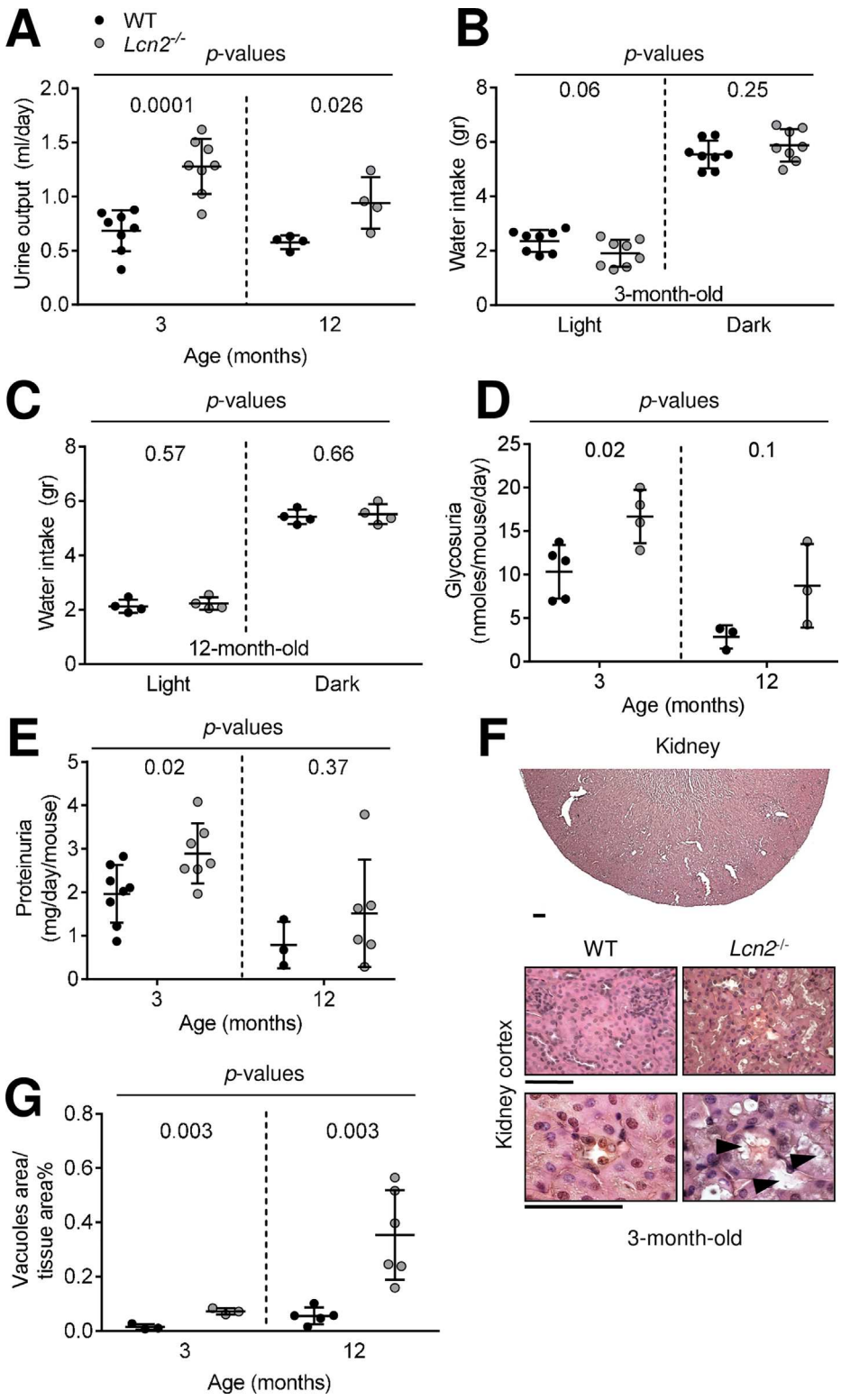

Fig. 6. Effect of *Lcn2* ablation on renal functions. Three-month-old and 12-month-old WT and *Lcn2*$^{-/-}$male mice were housed in metabolic cages to assess (*A*) urine output and (*B,C*) water intake. Evaluation of (*D*) glucose levels and (*E*) protein concentration in urine. (*F*) Histological sections of kidneys from WT and *Lcn2*$^{-/-}$ mice stained with hematoxylin/eosin and (*G*) evaluation of vacuolar area in the cortical region (unpaired Student's *t* test, number of mice/group = 3 to 8; scale bar = 25 μm). GTT = glucose tolerance test; ITT = insulin tolerance test.

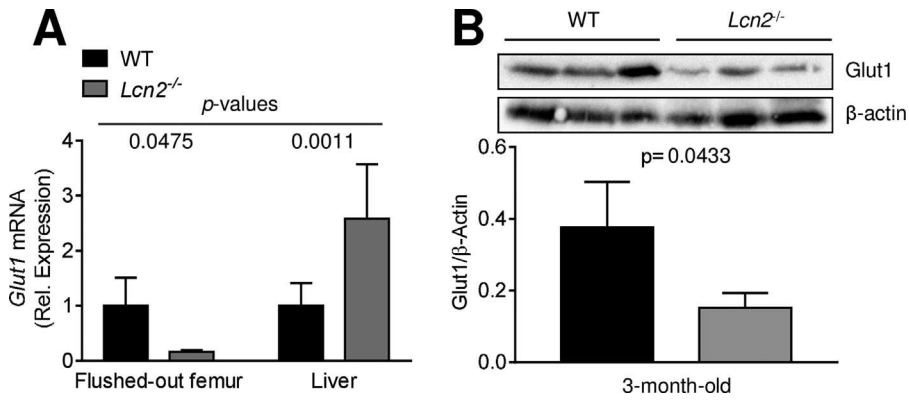

Fig. 7. Glut1 expression. (*A*) Transcriptional expression of *Glut 1* in the indicated tissues. (*B*) Western blot analysis of GLUT 1 in marrow flushed-out femurs (unpaired Student's *t* test, number of mice/group = 3 to 5).

hyperinsulinemia can promote obesity,[30–33] whereas drugs that prevent hyperinsulinemia can lead to weight loss.[33,34] Given that the insulin sensitivity in *Lcn2*$^{-/-}$ mice was normal, hyperinsulinemia could indeed account for the higher glucose tolerance and fasted hypoglycemia observed in *Lcn2*$^{-/-}$ mice. However, a previous study showed that Lcn2 deficiency reduced glycemia and insulinemia, and enhanced insulin sensitivity in aging, dietary or genetic-induced obesity,[6] partly diverging from our observations and corroborating the observations by Mosialou and colleagues.[11]

To make the phenotype even more complex, glucose excretion and kidney function appeared altered in our *Lcn2*$^{-/-}$ mice. Lcn2 is very important for the iron handling and recycling in the kidney, preventing iron accumulation in tubular kidney cells.[35] Lcn2 has also been proposed as a biomarker of acute kidney injury[36] and our data showed that *Lcn2*$^{-/-}$ kidneys presented with proteinuria and cortex vacuolization, which is morphologically consistent with iron-induced kidney injury.[35] This could also potentially be the cause of the polyuria and glycosuria, which could contribute to the circulating glucose depletion in *Lcn2*$^{-/-}$ mice.

The mechanisms underlying the response of the bone to the Lcn2-induced hypoglycemia and hyperinsulinemia remain to be fully elucidated, representing a limitation of our study. The basal insulin receptor and downstream signaling pathways appeared similar in WT and *Lcn2*$^{-/-}$ mice. However, the expression of GLUT1 in the bone was downregulated in *Lcn2*$^{-/-}$ mice. GLUT1 transports glucose in osteoblasts, and glucose uptake stimulates osteoblast differentiation through a mechanism that stabilizes Runx2 by preventing its degradation into the proteasome.[26] Glucose uptake by osteoblasts is independent of insulin, and in osteoblasts GLUT1 has been demonstrated to be more expressed compared to other glucose transporters.[26] Mouse genetics showed that GLUT1 expression is enhanced by Runx2 and that Runx2 cannot induce osteoblast differentiation in the presence of low glucose. Therefore, it is conceivable, although rather speculative, that the impairment of GLUT1 expression in *Lcn2*$^{-/-}$ bone could contribute to the low bone formation observed in these mice.

In conclusion, Lcn2 is a very peculiar protein, whose physiologic level appears to be essential for bone health, balanced energy metabolism, and normal kidney function. Together with other reports,[11,23,24] we have highlighted that the pathways in which Lcn2 is involved are very complex and not yet fully understood. It should be noted that Lcn2 is also called growth factor super-inducible protein 24[37] because of its strong transcriptional activation in various conditions. Therefore, we cannot rule out that small experimental or environmental differences could also be responsible for the discrepancies noted in various studies. Furthermore, strategies to generate the available Lcn2 mouse models were different, for instance deleting a 1.9-kilobase (kb) genomic fragment comprising *Lcn2* exons 3 to 6 by LoxP sites within introns 2 and 6 in Mosialou and colleagues,[11] or using a targeting vector designed to replace a 2.5-kb genomic fragment containing Lcn2 exons 1 to 5 with the PGK-neo cassette in Berger and colleagues,[12] who generated the mice investigated in this study. Therefore, further research and controlled approaches will be necessary to recognize the exact multifaceted roles of Lcn2 in the organismal health, elucidate the underlying cellular and molecular mechanisms and reconcile the many divergent observations reported so far in the literature (Supporting Table 1).

Disclosures

All authors state that they have no conflicts of interest.

Acknowledgments

This work was supported by the STRODER-SIOMMMS grant to NR, and two the European Commission grants to AT: – Program "PEOPLE" – Call identifier: FP7-PEOPLE-2011-IRSES – Proposal No. 295181 – Acronym: INTERBONE; and Program "Collaborative Project – Large-scale integrating project" – Call identifier: FP7-HEALTH.2012.2.1.1-1-C Proposal No. 602300 – Acronym: SYBIL. We are indebted to Dr. Rita Di Massimo for her excellent contribution in writing this manuscript.

Authors' roles: Study design: NR, MC, AM, MP, and AT. Study conduct: NR, MC, MP, AM, and SGP. Data collection: NR, MC, AM, MP, SGM, and AT. Data analysis: NR, MC, AM, MP, SGM, and AT. Data interpretation: NR, MC, AM, MP, and AT. Mouse generation: TWM and TB. Manuscript drafting: NR, MP, and AT. Manuscript revision: NR, MP, and AT. Approving of final manuscript: NR, MC, AM, MP, SGP, PL, TWM, TB, and AT.

References

1. Lögdberg L, Wester L. Immunocalins: a lipocalin subfamily that modulates immune and inflammatory responses. Biochim Biophys Acta. 2000;1482:284–97.
2. Abella V, Scotece M, Conde J, et al. The potential of lipocalin-2/NGAL as biomarker for inflammatory and metabolic diseases. Biomarkers. 2015;20:565–71.
3. Zhang Y, Foncea R, Deis AJ, Guo H, Bernlohr DA, Chen X. Lipocalin 2 expression and secretion is highly regulated by metabolic stress, cytokines, and nutrients in adipocytes. PLoS One. 2014;9:1–9.
4. Guo H, Jin D, Zhang Y, et al. Lipocalin-2 deficiency impairs thermogenesis and potentiates diet-induced insulin resistance in mice. Diabetes. 2010;59:1376–85.
5. Guo H, Zhang Y, Brockman DA, Hahn W, Bemhlor DA, Chen X. Lipocalin 2 deficiency alters estradiol production and estrogen receptor signaling in female mice. Endocrinology. 2012;153(3):1183–93.
6. Law IKM, Xu A, Lam KSL, et al. Lipocalin-2 deficiency attenuates insulin resistance associated with aging and obesity. Diabetes. 2010;59:872–82.
7. Jin D, Guo H, Bu SY, et al. Lipocalin 2 is a selective modulator of peroxisome proliferation-activated receptor-γ activation and function in lipid homeostasis and energy expenditure. FASEB J. 2011;25:754–64.
8. Paton CD, Rogowski MP, Kozimor AL, Stevenson JL, Chang H, Cooper JA. Lipocalin-2 increases fat oxidation in vitro and is correlated with energy expenditure in normal weight but not obese women. Obesity. 2013;21:E640–8.
9. Capulli M, Rufo A, Teti A, Rucci N. Global transcriptome analysis in mouse calvarial osteoblasts highlights sets of genes regulated by modeled microgravity and identifies a "mechanoresponsive osteoblast gene signature". J Cell Biochem. 2009;107:240–52.
10. Rucci N, Capulli M, Piperni-Gemini S, et al. Lipocalin 2: a new mechanoresponding gene regulating bone homeostasis. J Bone Miner Res. 2015;30:357–68.
11. Mosialou I, Shikhel S, Liu JM, et al. MC4R-dependent suppression of appetite by bone-derived lipocalin 2. Nature. 2017;543:385–90.
12. Berger T, Togawa A, Duncan GS, et al. Lipocalin 2-deficient mice exhibit increased sensitivity to Escherichia coli infection but not to ischemia-reperfusion injury. Proc Natl Acad Sci U S A. 2006; 103:1834–9.
13. Feldkamp LA, Davis LC, Kress JW. Practical cone-beam algorithm. J Opt Soc Am. 1984;1:612–9.
14. Lorensen WE, Cline HE. Marching cube: a high resolution 3d surface construction algorithm. SIGGRAPH Comput Graph. 1987;21:163–9.
15. Pratt WT. *Digital image processing*. 2nd ed. New York: Wiley; 1991.
16. Bouxsein ML, Boyd SK, Christiansen BA, Guldberg RE, Jepsen KJ, Müller R. Guidelines for assessment of bone microstructure in rodents using micro-computed tomography. J Bone Miner Res. 2010;25:1468–86.
17. Rucci N, Rufo A, Alamanou M, et al. The glycosaminoglycan-binding domain of PRELP acts as a cell type-specific NF-kappaB inhibitor that impairs osteoclastogenesis. J Cell Biol. 2009;187:669–83.
18. Dempster DW, Compston JE, Drezner MK, et al. Standardized nomenclature, symbols and units for bone histomorphometry: a 2012 update of the report of the ASBMR Histomorphometry Nomenclature Committee. J Bone Miner Res. 2013;28:2–17.
19. Li DS, Yuan YH, Tu HJ, Liang QL, Dai LJ. A protocol for islet isolation from mouse pancreas. A protocol for islet isolation from mouse pancreas. Nat Protoc. 2009;4:1649.
20. Ellacott KLJ, Morton GJ, Woods SC, Tso P, Schwartz MW. Assessment of feeding behavior in laboratory mice. Cell Metab. 2010;12:10–7.
21. Veeriah V, Zanniti A, Paone R, et al. Interleukin-1β, lipocalin 2 and nitric oxide synthase 2 are mechano-responsive mediators of mouse and human endothelial cell-osteoblast crosstalk. Sci Rep. 2016;6:29880.
22. Hyun-Ju K, Boram O, Woo-Youl K, et al. Deficiency of lipocalin-2 promotes proliferation and differentiation of osteoclast precursors via regulation of c-Fms expression and nuclear factor-kappa B activation. J Bone Metab. 2016;23:8–15.
23. Ferron M, Wei J, Yoshizawa T, et al. Insulin signaling in osteoblasts integrates bone remodeling and energy metabolism. Cell. 2010;142:296–308.
24. Fulzele K, Riddle RC, DiGirolamo DJ, et al. Insulin receptor signaling in osteoblasts regulates postnatal bone acquisition and body composition. Cell. 2010;142:309–19.
25. Viau A, E1 Karoui K, Laouari D, et al. Lipocalin 2 is essential for chronic kidney disease progression in mice and humans. J Clin Invest. 2010;120:4065–76.
26. Wei J, Shimazu J, Makinistoglu MP, et al. Glucose uptake and Runx2 synergize to orchestrate osteoblast differentiation and bone formation. Cell. 2015;161:1576–91.
27. Mastaitis JW, Wurmbach E, Cheng H, Sealfon SC, Mobbs CV. Acute induction of gene expression in brain and liver by insulin-induced hypoglycemia. Diabetes. 2005;54:952–8.
28. Tsai TL, Li WJ. Identification of bone marrow-derived soluble factors regulating human mesenchymal stem cells for bone regeneration. Stem Cell Rep. 2017;8:387–400.
29. Wang Y. Small lipid-binding proteins in regulating endothelial and vascular functions: focusing on adipocyte fatty acid binding protein and lipocalin-2. Br J Pharmacol. 2012;165:603–21.
30. Templeman NM, Skovso S, Page MM, Lim GE, Johnson JD. A causal role for hyperinsulinemia in obesity. J Endocrinol. 2017;232:R173–83.
31. Corkey BE. Banting lecture 2011: hyperinsulinemia: cause or consequence? Diabetes. 2012;61:4–13.
32. Odeleye OE, de Courten M, Pettitt DJ, Ravussin E. Fasting hyperinsulinemia is a predictor of increased body weight gain and obesity in Pima Indian children. Diabetes. 1997;46:1341–5.
33. Lustig RH, Greenway F, Velasquez-Mieyer P, et al. A multicenter, randomized, double-blind, placebo-controlled, dose-finding trial of a long-acting formulation of octreotide in promoting weight loss in obese adults with insulin hypersecretion. Int J Obes. 2015;30:331–41.
34. Alemzadeh R, Jacobs W, Pitukcheewanont P. Antiobesity effect of diazoxide in obese zucker rats. Metabolism. 1996;45:334–41. 32.
35. Schmidt-Ott KM, Mori K, Kalandadze A, et al. Neutrophil gelatinase-associated lipocalin-mediated iron traffic in kidney epithelia. Curr Opin Nephrol Hypertens. 2006;15:442–9.
36. Konno T, Nakano R, Mamiya R, et al. Expression and function of interleukin-1β-induced neutrophil gelatinase-associated lipocalin in renal tubular cells. PLoS One. 2016;11:e0166707.
37. Liu QS, Nilsen-Hamilton M, Xiong SD. Synergistic regulation of the acute phase protein SIP24/24p3 by glucocorticoid and pro-inflammatory cytokines. Sheng Li Xue Bao. 2003;55:525–9.